Coordinated Control Strategy for Operation Mode Switching of DC Distribution Networks

Jianqiang Liu, Xiaoguang Huang, Ying Hong, and Zuyi Li

***Abstract*—Due to the advantages such as low line cost, low transmission loss, and high power supply reliability, DC distribution networks have become the main development trend for future distribution networks. In this paper, a typical DC distribution network with multiple voltage levels is considered as a research object. It is proposed that the interface converters between DC buses with different voltage levels be implemented through the series-parallel combination of full-bridge LLC resonant converters. To realize the decentralized self-discipline control of DC voltage under various working conditions, different slack buses are prepared according to the voltage ranges of the DC buses, and the voltage regulation modes of the DC distribution network are divided into main voltage regulation mode, backup voltage regulation mode, and off-grid voltage droop regulation mode. By introducing a voltage coefficient related to DC voltage deviation as a basis for mode switching, the voltage fluctuations caused by slow switching between control modes in the method of traditional voltage margin control is reduced, facilitating fast and smooth switching between different voltage regulation modes. Finally, a simulation model for DC distribution networks is constructed utilizing MATLAB/Simulink. Simulation results verify the effectiveness and feasibility of the proposed voltage regulation modes and switching methods for DC distribution networks. Finally, an experimental platform is also constructed to verify the feasibility of the mode switching method proposed in this paper.**

***Index Terms*—DC distribution network, decentralized self-discipline control, voltage regulation mode, mode switching.**

I. Introduction

BASED on the combined crises of environmental pollution and fossil energy shortages, renewable energy has become a major focus. Therefore, energy infrastructures will experience profound changes in the future. However, renewable energy sources such as wind power and solar energy, have the characteristics of indirectness, randomness, and volatility, meaning traditional AC power distribution systems encounter significant issues when large numbers of renewable energy sources are connected to the grid [1]. Based on the continued development of power electronic technology and power semiconductors, maturity of high-voltage direct current (HVDC) transmission technology, and implementation of low-voltage direct current (LVDC) microgrids and DC power supply technology, more reliable, efficient, environmentally friendly, and economical DC distribution networks have exhibited several advantages in certain areas [2]-[7].

The key to the stable operation of DC distribution systems is the stability of DC bus voltage. The control objective is to coordinate power exchange between sources and loads effectively within a DC distribution system by implementing a reasonable coordination control mechanism so that the DC voltage can be stabilized within a certain range. The research on DC bus voltage control is relatively mature and various control schemes have been developed, including master-slave control [8], [9], voltage margin control [10], voltage droop control [11], [12], and hybrid control strategies [13]-[15]. Although master-slave control has the advantages of desirable control characteristics and high DC voltage quality, power can move out of balance and DC voltage becomes uncontrollable when the master station is out of operation. Additionally, such systems have strict requirements in terms of communication. DC voltage margin control does not depend on communication and has high reliability, but voltage fluctuations are large when the mode is switched. Voltage droop control has strong regulation ability, but it cannot achieve precise voltage control. In [14], a novel control strategy combining voltage margin control with voltage droop control is proposed to leverage the advantages of each control methods and compensate for their shortcomings. However, this system still encounters the problem of oscillation when voltage margin selection is inappropriate. Tradeoff coefficients related to DC voltage deviation are set to switch the control mode of the margin controller so that the response speed and adjustment speed of the controller are accelerated when the DC voltage deviation of the system is large [15]-[17], but the design of the controller and selection of tradeoff coefficients are complicated. This is because the smooth switching between different modes depends entirely on the trade-off coefficients, which are calculated based on complex hyperbolae.

Similar to AC distribution networks, future DC distribution systems must engage in mutual cooperation to realize multi-level DC distribution networks. In this paper, a typical DC distribution network with high, medium, and low volt-

Manuscript received: October 31, 2018; accepted: October 17, 2019. Date of CrossCheck: October 17, 2019. Date of online publication: February 28, 2020.

This work was supported by Fundamental Research Funds for the Central Universities (No. 2019JBM057).

J. Liu (corresponding author), X. Huang, and Y. Hong are with the School of Electrical Engineering, Beijing Jiaotong University, Beijing 100044, China (e-mail: liujianqiang@bjtu.edu.cn; huangxiaoguang80@163.com; 16121453@bjtu.edu.cn).

Z. Li is with Robert W. Galvin Center for Electricity Innovation, Illinois Institute of Technology, Chicago 60616, USA (e-mail: lizu@iit.edu).

DOI: 10.35833/MPCE.2018.000780

age levels is considered as a research object. A novel mode switching method (NMSM) is proposed for the DC distribution network, which has many operation modes. The NMSM can realize automatic switching between different voltage regulation modes by introducing coefficients related to DC bus voltage deviation. Compared to traditional voltage margin control (TVMC), NMSM proposed in this paper makes switching between voltage regulation modes faster and reduces fluctuations in voltage and power during the transition process.

The remainder of this paper is organized as follows. Section II introduces the architecture of a typical DC distribution network and an interface converter for switching between different DC buses. Section III proposes three different voltage regulation modes for operating the DC distribution network to ensure the stability of DC bus voltage under any operation conditions. Section IV analyzes the deficiencies of TVMC. On the basis of this analysis, a fast mode switching method based on voltage coefficients is proposed to realize automatic switching between different voltage regulation modes. Section V presents simulations verifying the feasibility and effectiveness of the voltage regulation modes and NMSM. Section VI concludes this paper.

II. Composition of DC Distribution Network System

A typical ring DC distribution network with multi-stage bus interconnections is presented in Fig. 1.

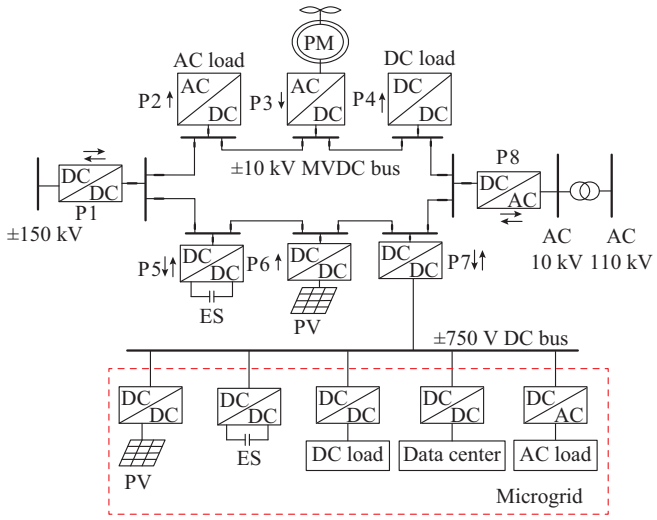

Fig. 1. Topology of a ring DC distribution network.

The system is mainly composed of the following four parts.

1) Main network converters. The main network converters include P1 and P8. P8, which is the voltage source converter (VSC), is the interface converter for the 110 kV high-voltage alternating current (HVAC) main network and ±10 kV medium-voltage direct current (MVDC) distribution network. P1 is the interface converter between the ±150 kV HVDC main grid and MVDC distribution network. Since the conversion of DC voltage cannot be realized through electromagnetic induction, unlike AC systems, a power converter based on power electronics technology must be utilized to realize voltage conversion and energy transfer. In the proposed system, DC/DC interface converters between the DC buses of different voltage levels are formed based on the series-parallel combination of full-bridge LLC resonant converters [18], [19], as shown in Fig. 2(a). In consideration of the applications with high-voltage inputs and medium-voltage outputs, P1 adopts an input-series output-series structure, as shown in Fig. 2(b).

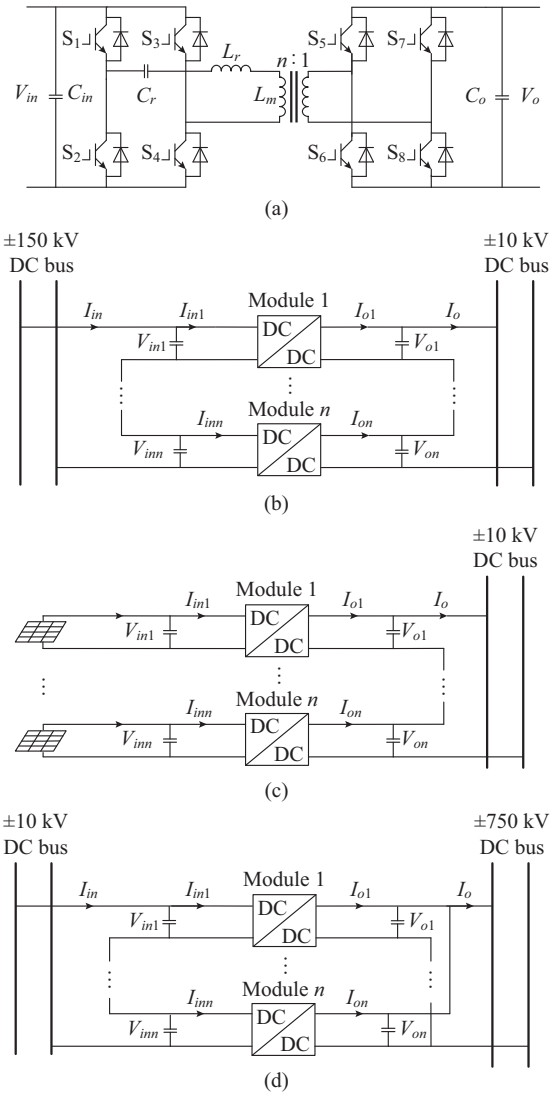

Fig. 2. DC/DC interface converter. (a) Schematic diagram of LLC resonant converter circuit. (b) Interface converter between HVDC and MVDC buses. (c) PV grid-connected converter. (d) Interface converter between MVDC and LVDC buses.

2) Renewable energy generation unit. Wind farms and photovoltaic (PV) cells are connected to the DC side via the VSC (P3) and DC/DC converter (P6), respectively. Since the output voltage of the PV array is approximately 600 V, the PV grid-connected converter is implemented with a combined structure, as shown in Fig. 2(c). Since the power of the PV station is unidirectional, the secondary-side switches of the LLC resonant converter can be replaced with diodes.

3) Energy storage (ES) unit. The ES unit is connected to the MVDC side through a bidirectional DC/DC converter (P5). However, supercapacitors face the issue of low-voltage levels. Therefore, in this study, by considering the LLC resonant converter as a standard module, the energy conversion scheme for the ES system presented in Fig. 2(c) is adopted for medium-voltage applications (the PV cells are replaced with supercapacitors in Fig. 2(c)). When ES is discharged, converter power flows in the forward direction to supply power to the DC bus. When ES is charged, the converter power flows in reverse to store the excessive power from the DC bus.

4) Loads. Loads include both AC loads and DC loads. AC loads are connected to the MVDC bus through VSC (P2). DC loads and the ±750 V LVDC distribution network are connected to the MVDC distribution network through an input-series output-parallel structure, as shown in Fig. 2(d). The DC/DC modules still utilize LLC resonant converters with good soft switching performance and high power density.

In the proposed system, a large number of interface converters are utilized, which are combinations of series and parallel connections with LLC resonant converters as standard modules. This not only reduces the thermal and electrical stress on power devices and improves system reliability, but also shortens the development cycle for the system, thereby reducing the development costs.

III. Voltage Regulation Modes of DC Distribution Network

Similar to an AC distribution network, the control technology in DC distribution networks can be divided into three levels: distribution network level, microgrid level, and unit level. The structure of a DC distribution network is illustrated in Fig. 3.

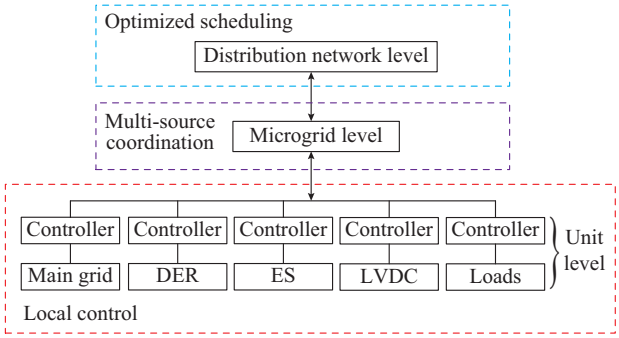

Fig. 3. Control structure of a DC distribution network.

Based on various data such as distributed generation power predictions, load demands, ES operation status, and market information, and according to different optimal operation objectives and constraints, the purpose of control on the distribution network level is to formulate a DC grid operation scheduling strategy in real time so that safe and economical operation of the system can be guaranteed. Voltage drops along the main line and network loss are considered at this control level.

In a DC distribution network, there are many types of power supplies with different degrees of controllability, so there are many operation states in such a system. The control objective at the microgrid level is to ensure coordinated control of power supplies and loads in a DC distribution network. DC bus control tasks are assigned to converters according to various working conditions of the distribution network to maintain DC bus voltage stability and power balance of the system. The microgrid level is the main focus of this paper.

The unit level is responsible for the basic control of power electronic converters. Based on local information, the voltage, power, and current of each unit are regulated to ensure normal operation.

When the load power changes or the maximum power of distributed generation units changes according to the environmental conditions, or if the state of charge of the ES station changes or the main network converter fails, the DC bus voltage will rise or drop accordingly. In such cases, each unit must change its control strategy according to a preset state so the system can switch to the next operation mode.

In any operation mode, the system should have a corresponding converter station acting as a slack bus to maintain the stability of the DC bus voltage. In this paper, according to the range of DC bus voltage and the voltage regulation capability of the converter station, voltage regulation for a DC distribution network is divided into the main voltage regulation mode, backup voltage regulation mode, and off-grid voltage droop regulation mode. These regulation modes are defined as follows.

1) The main voltage regulation mode is the normal working mode of the system. In this mode, P8 acts as the slack bus for the DC distribution network and controls the DC bus voltage. P1 either provides constant DC power or stops running. Renewable energy generation units are controlled by a maximum power point tracking (MPPT) scheme to achieve maximum energy utilization. To ensure that the ES unit can supply energy to the system continuously in off-grid mode, ES unit P5 operates in a current-limiting charging or shutdown state in the main voltage regulation mode. A control block diagram for each converter in the main voltage regulation mode is presented in Fig. 4.

Figure 4(b) presents the power control strategy for P1. The control strategy is divided into two parts: the output power loop controls the output DC power and the power balance control maintains the power balance of each module. Under power control, DC bus voltages on both sides of the DC/DC interface converter remain stable. The basic switching frequency f_{bs} is equal to the output of a proportional-integral (PI) controller, whose input is a comparison between the actual output power and reference value of the output power. Next, f_{bs} is combined with Δf_i ($i = 1, 2, \ldots, n$), which is the output of the power balance controller, to obtain the final switching frequency f_s for each module. In this manner, the output power is adjusted, and the output power equalization of each module is achieved. PV and wind power systems utilize MPPT to maximize the utilization of renewable energy, as shown in Fig. 4(c) and (d). Since the DC/DC con-

verter module of the PV grid-connected converter is an LLC resonant converter, MPPT can be achieved by adjusting the switching frequency. In Fig. 4(d), the PV current i_{PV} and PV voltage V_{PV} generate a voltage reference value V_{ref} after passing through the MPPT controller. The basic switching frequency of the PV station is the output of the PI regulator, whose input is the difference between V_{PV} and V_{ref}.

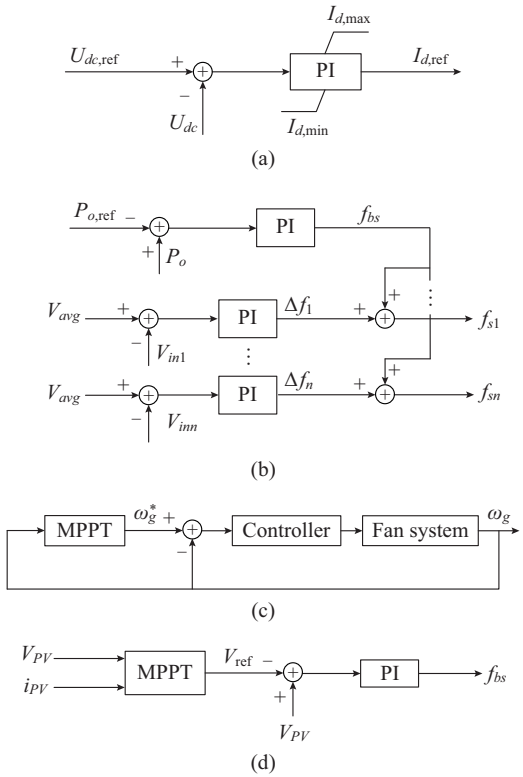

Fig. 4. Control block diagrams of each converter in main voltage regulation mode. (a) Control block diagram of P8. (b) Control block diagram of P1. (c) Control block diagram of P3. (d) Control block diagram of P6.

In the main voltage regulation mode, the DC bus voltage U_{dc} satisfies:

$$U_{n1} \le U_{dc} \le U_{m1} \tag{1}$$

where U_{m1} and U_{n1} are the upper and lower limits of the DC bus voltage during normal operation of the system, respectively. When the renewable energy or load power changes, if the DC bus voltage fluctuation does not exceed this range, the system continues to run in the main voltage regulation mode.

2) When the output power of P8 reaches the limit or P8 fails, the system switches to backup voltage regulation mode. In this mode, P8 loses the ability to control DC voltage and P1 is utilized as a new slack bus to control DC voltage. Renewable energy generation units continue to operate in the MPPT state and the ES unit operates in a charging or discharging state according to the maximum power of the renewable energy generation units and the load power. The control strategy for each converter in the backup voltage regulation mode is similar to that in the main voltage regulation mode. The differences are that: ① P8 operates at limited power or does not exchange power with the DC network; ② P1 performs constant DC voltage control, which is also divided into two parts. The output voltage loop stabilizes the DC voltage and the power balance control maintains the power balance of each module. The final switching frequency of each module is a combination of the balance correction amount Δf and basic switching frequency f_{bs}, which is regulated by the output voltage error signal.

In the backup voltage regulation mode, the DC bus voltage satisfies (2) or (3).

$$U_{n2} \le U_{dc} < U_{n1} \tag{2}$$

$$U_{m1} < U_{dc} \le U_{m2} \tag{3}$$

where U_{m2} and U_{n2} are the upper and lower limits of the DC bus voltage in backup voltage regulation mode, respectively. When all converters connected to the upper public main network are out of operation, the DC bus voltage will increase or decrease. If the DC bus voltage is higher than U_{m2} or lower than U_{n2}, the control of the renewable energy generation units is switched from MMPT control to voltage droop control.

3) When the circuit breakers connected to the two public main grids are disconnected, the system switches to off-grid voltage droop regulation mode. In this mode, there is no power exchange between the system and the public main network, and only the distributed generation and load systems are in operation. At this point, all renewable energy generation units switch to voltage droop control to maintain the stability of the DC bus voltage and the power balance of the system. If the distributed generation units cannot meet the power demands of the loads, then non-important loads should be removed to maintain an energy balance and stabilize the DC bus voltage. A control block diagram for each converter in the off-grid droop regulation mode is presented in Fig. 5.

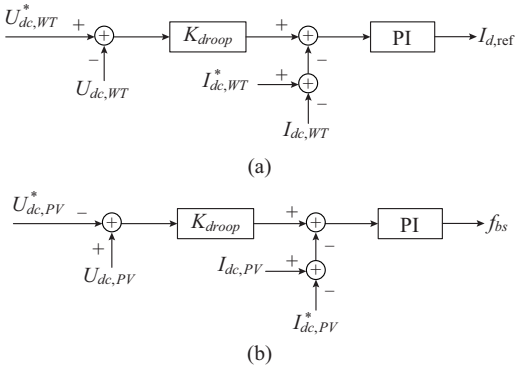

Fig. 5. Control block diagrams of each type of converter in off-grid voltage droop regulation mode. (a) Control block diagram of P3. (b) Control block diagram of P6.

In Fig. 5, $U_{dc,WT}$ and $U_{dc,PV}$ are the grid-connected port voltages of P3 and P6, respectively; $I_{dc,WT}$ and $I_{dc,PV}$ are the corresponding grid-connected currents; the superscript $*$ represents the reference value of corresponding variable; $I_{d,\text{ref}}$ is the d-axis reference current of P3; and K_{droop} is the voltage droop coefficient.

IV. Mode Switching Method

A. TVMC

Based on the analysis above, it can be seen that the proposed system has three different voltage regulation modes. When the power fluctuations of loads or renewable energy generation units are large or the main network equipment is out of control, the operation mode of the system changes. When the system operation mode changes, the control modes for some grid-connected converters may need to be adjusted accordingly to different voltage regulation modes to maintain the stability of the DC bus voltage. Therefore, it is necessary to develop appropriate criteria for switching between different voltage regulation modes and appropriate methods for coping with changes in the operation mode of the DC distribution system.

Mode switching under TVMC does not need to rely on rapid communication because one can preset the DC voltage margin value for each converter station and monitor local information, allowing each converter station to change control modes automatically according to the magnitude of the DC voltage. However, the system does not change control mode immediately under TVMC when the DC voltage exceeds a preset value. In this study, the main voltage regulation mode is switched to the backup voltage regulation mode as an example for detailed analysis. The control process of the converter station (P1) based on the TVMC strategy is presented in Fig. 6.

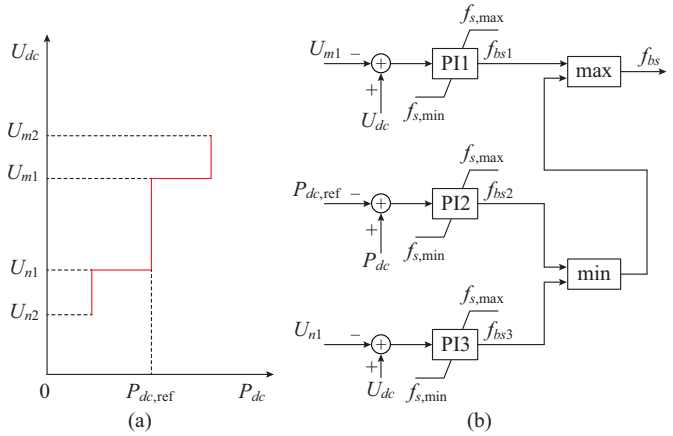

Fig. 6. Process for TVMC. (a) U_{dc}-P_{dc} characteristics of P1. (b) Controller structure of P1.

In Fig. 6, U_{m1} and U_{n1} are preset based on the DC voltage margin; $P_{dc,ref}$ is the power reference value of a margin controller operating in constant power control mode; and f_{bs1}, f_{bs2}, and f_{bs3} are the outputs of PI1, PI2, and PI3, respectively, which correspond to the fundamental switching frequency in Fig. 4(b). Since P1 with the voltage margin controller adopts frequency conversion control, the automatic switching between control modes is realized by checking the relative magnitudes of the basic switching frequency output by each PI regulator.

When a DC distribution system operates in the main voltage regulation mode, the DC bus voltage is controlled by the AC/DC converter P8, which is connected to the AC main grid. In this voltage regulation mode, the DC bus voltage range is:

$$U_{n1} < U_{dc} < U_{m1} \tag{4}$$

Therefore, the relative magnitudes of the basic switching frequencies output by each PI regulator can be written as follows:

$$f_{bs1} = f_{s,\min} < f_{bs2} < f_{s,\max} = f_{bs3} \tag{5}$$

This means that P1 connected to the upper-level DC distribution network operates in constant DC power control mode with a basic switching frequency equal to the output of PI2.

When P8 is out of operation as a result of fault or maintenance, the DC bus voltage U_{dc} increases or decreases based on system power imbalances. If P8 is in the state of injecting power into the DC power distribution system before its operation ends, U_{dc} will drop after P8 stops the operation. When U_{dc} falls below the minimum value of the voltage margin U_{n1}, f_{bs3} will gradually decrease from $f_{s,\max}$. After a period of adjustment, the relative magnitudes of the basic switching frequency output by each PI regulator will change as follows:

$$f_{bs1} = f_{s,\min} < f_{bs3} < f_{bs2} \le f_{s,\max} \tag{6}$$

At this time, based on the control structure in Fig. 5, it can be seen that the basic switching frequency of converter P1 is:

$$f_{bs} = f_{bs3} \tag{7}$$

This indicates that the control of the converter P1 has changed from constant DC power to constant DC voltage, so the system switches to backup voltage regulation mode with the voltage reference value U_{n1}.

If P8 is in the state of absorbing power from the DC power distribution system before its operation ends, U_{dc} will increase after P8 stops operating. When U_{dc} increases to more than U_{m1}, the control mode of the converter P1 does not change immediately, but the output f_{bs1} of the regulator PI1 gradually increases from $f_{s,\min}$. Finally, the relative magnitudes of each PI regulator change as follows:

$$f_{s,\min} \le f_{bs2} < f_{bs1} < f_{s,\max} = f_{bs3} \tag{8}$$

At this point, P1 operates in constant DC voltage control mode with a voltage reference value U_{m1} and the system switches to backup voltage regulation mode.

Based on the above analysis, one can conclude that under TVMC, even if the DC bus voltage exceeds the system preset value, the control of P1 will not immediately change from constant power control mode to constant voltage control mode. Based on the adjustments by the PI regulator, the control mode will only switch when the relative magnitudes of basic switching frequency of each PI regulator change, which makes the mode switching process slower and increases the overall voltage fluctuation time.

B. Fast Mode Switching Method Based on Voltage Coefficient

To overcome the limitations of TVMC in terms of mode switching, a fast mode switching method based on voltage coefficient is proposed. We determine the operation mode of the converter by introducing a voltage coefficient K, which

is defined as:

$$K = \frac{U_{dc} - U_{dc,\mathrm{ref}}}{\Delta u} \tag{9}$$

where $U_{dc,\mathrm{ref}}$ is the DC bus voltage reference value, which is considered to be constant at 20 kV; and Δu is a switching threshold of preseted control mode that defines how much the DC bus voltage is allowed to deviate from the reference value in the main voltage regulation mode. When the DC distribution system in Fig. 1 operates in the main voltage regulation mode, P1 operates in the constant DC power control mode. At this time, $-1 < K < 1$. If P8 is out of operation, U_{dc} increases. When it increases to more than $U_{dc,\mathrm{ref}} + \Delta u$, $K \geq 1$ and P1 switches to the constant DC voltage control mode. If P8 is out of operation, U_{dc} decreases. When it falls below $U_{dc,\mathrm{ref}} - \Delta u$, $K \leq -1$ and P1 switches to the constant DC voltage control mode. To prevent the control mode from changing rapidly near the switching threshold, the voltage reference value for the constant voltage control mode has the following relationship with the switching threshold:

$$\begin{cases} U_{m1} > U_{dc,\mathrm{ref}} + \Delta u \\ U_{n1} < U_{dc,\mathrm{ref}} - \Delta u \end{cases} \tag{9}$$

When the DC bus voltage deviation exceeds Δu, P1 first utilizes slope control to give the DC voltage a drooping characteristic, thereby reducing the impact of the converter P1 suddenly taking over DC voltage control. If the DC voltage changes too much, i.e., the output voltage of P1 is out of the range between U_{n1} and U_{m1}, constant voltage control is utilized to prevent the DC voltage from continuously deviating from the rated value. A novel mode switching method that improves upon the TVMC is presented in Fig. 7.

In Fig. 7, $U_{o,\mathrm{ref}}$ is the voltage reference value of the voltage regulator. In different scenarios, $U_{o,\mathrm{ref}}$ will vary. When the voltage regulator is in the main voltage mode, i.e., $-1 < K < 1$,

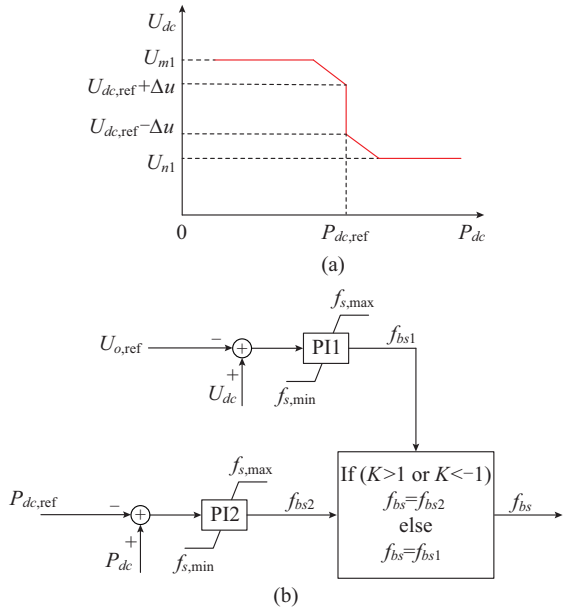

Fig. 7. Control strategy for the proposed fast mode switching method based on a voltage coefficient. (a) U_{dc}-P_{dc} characteristics of P1. (b) Controller structure of P1.

$$U_{o,\mathrm{ref}} = \begin{cases} U_{dc} - G & f_{bs1} < f_{bs2} \\ U_{dc} & f_{bs1} = f_{bs2} \end{cases} \tag{10}$$

When $K \geq 1$,

$$U_{o,\mathrm{ref}} = \begin{cases} U_{m1} + \dfrac{I_{dc,\mathrm{ref1}} - I_d}{K_{droop}} & K < \dfrac{U_{m1} - U_{dc,\mathrm{ref}}}{\Delta u_1} \\ U_{m1} & K \geq \dfrac{U_{m1} - U_{dc,\mathrm{ref}}}{\Delta u_1} \end{cases} \tag{11}$$

When $K \leq -1$,

$$U_{o,\mathrm{ref}} = \begin{cases} U_{n1} + \dfrac{I_{dc,\mathrm{ref2}} - I_d}{K_{droop}} & K > \dfrac{U_{n1} - U_{dc,\mathrm{ref}}}{\Delta u_1} \\ U_{n1} & K \leq \dfrac{U_{n1} - U_{dc,\mathrm{ref}}}{\Delta u_1} \end{cases} \tag{12}$$

where G is a constant based on the output voltage, which ensures that the output of PI2 quickly matches that of PI1 in the main voltage regulation mode, i.e., the output of the voltage regulator PI2 can effectively avoid slow adjustments based on the limit value after changing control modes, thereby accelerating the adjustment process; Δu_1 is the switching threshold of P1 control mode; I_d is the DC current based on local information detection; and $I_{dc,\mathrm{ref1}}$ and $I_{dc,\mathrm{ref2}}$ are the reference values for DC current.

By introducing the voltage coefficient K to trigger switching between control modes, once the DC bus voltage is out of range, a converter P1 with the NMSM immediately switches to voltage control mode. The process of changing the relative magnitudes of each PI regulator output under TVMC is omitted, which accelerates the switching process and makes the system recover more quickly.

The controller structures of PV stations under TVMC and NMSM are presented in Fig. 8. When the operation mode of such a system changes abruptly, it will be faster and smoother to switch from the main voltage regulation mode or backup voltage regulation mode to the off-grid voltage droop regulation mode under NMSM than under TVMC.

V. Simulations and Experimental Verification

To verify the effectiveness of the proposed voltage regulation modes and the related switching control strategy, the DC distribution system in Fig. 1 is modeled in MATLAB/Simulink. The main parameters for the simulation system are listed in Table I.

A. Steady-state Simulation in Different Voltage Regulation Modes

Under normal working conditions, the system adopts the main voltage regulation mode. P8 operates in constant DC voltage control mode with a voltage reference value of 20 kV. P1 performs constant DC power control with a power command value of 5 MW. P3 and P6 have maximum power values of 8 MW and 9 MW, respectively, prior to t = 1 s, which change to 5 MW and 6 MW, respectively, when t = 1 s. The simulation results are presented in Fig. 9.

Figure 10 presents the simulation results in backup voltage regulation mode with P1 operating in constant DC volt-

age control mode with a voltage command value of 19.6 kV. P3 and P6 have maximum power values of 5 MW and 6 MW, respectively, prior to t = 1 s, which increase to 8 MW and 9 MW, respectively, when t = 1 s.

TABLE I
MAIN PARAMETERS FOR SIMULATION SYSTEM

Parameter	Value
Rated DC voltage $U_{dc,\mathrm{ref}}$ (kV)	20
Rated power of P1 and P8 (MW)	30
Lower and upper limits of reference voltage of P1 (kV)	19.6, 20.4
P1 control mode switching threshold Δu_1 (kV)	0.36
Rated power of P3 and P6 (MW)	10
Lower and upper limits of reference voltage of P3 and P6 (kV)	19.2, 20.8
Rated power of P2, P4, P5 and P7 (MW)	5

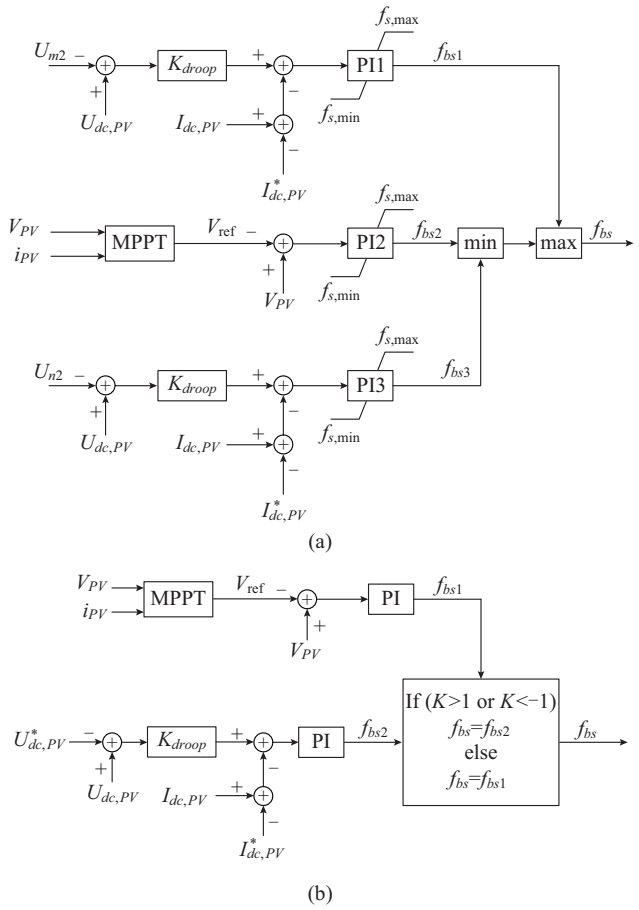

Fig. 8. Controller structures of PV stations. (a) Controller structure of a PV station under TVMC. (b) Controller structure of a PV station under NMSM.

When P1 and P8 are both out of operation, the system switches to off-grid voltage droop operation mode and the reference value of voltage command in the off-grid droop mode is determined by the output power of the wind farm or PV station in the previous stage. Figure 11 presents a steady-state simulation waveform of the off-grid droop mode with a voltage command value of 19.2 kV.

Since the output power of the wind farm or PV station can change at any time, the off-grid voltage droop mode is only suitable for the short-term operation. In Fig. 11, it is predicted that the maximum total output power of the wind farm and PV station are sufficient at 1 s, so the ES unit is switched from the discharging state to the charging state and the system stability can be maintained.

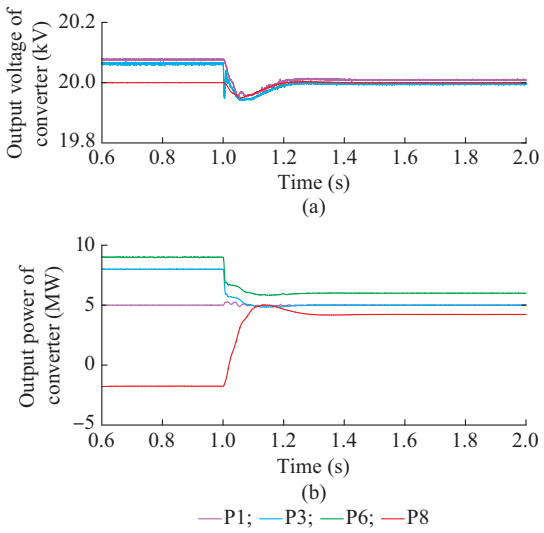

Fig. 9. Simulation waveforms under normal working conditions. (a) Output voltage waveforms. (b) Output power waveforms.

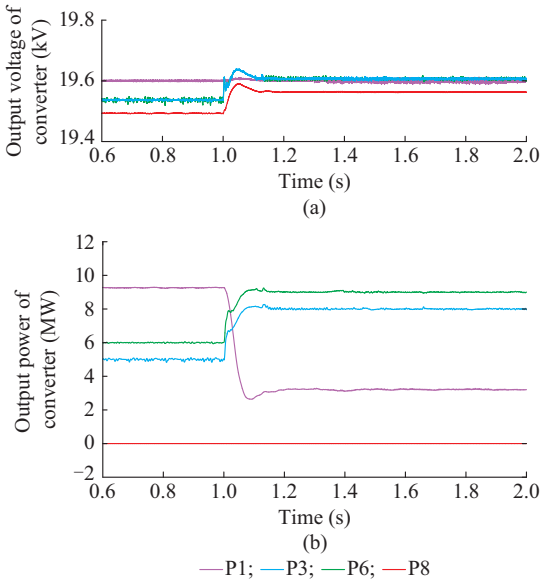

Fig. 10. Simulation waveforms in backup voltage regulation mode. (a) Output voltage waveforms. (b) Output power waveforms.

As shown in Figs. 9, 10, and 11, the system can operate stably in all three voltage regulation modes. When the maximum power of the wind farm or PV station changes, the power level or flow direction of the converter that controls the DC voltage changes in both the main voltage regulation mode and backup voltage regulation mode, but the system power balance can still be maintained. During this process,

voltage fluctuations are small and the switching threshold is not exceeded, so the voltage regulation mode is not switched.

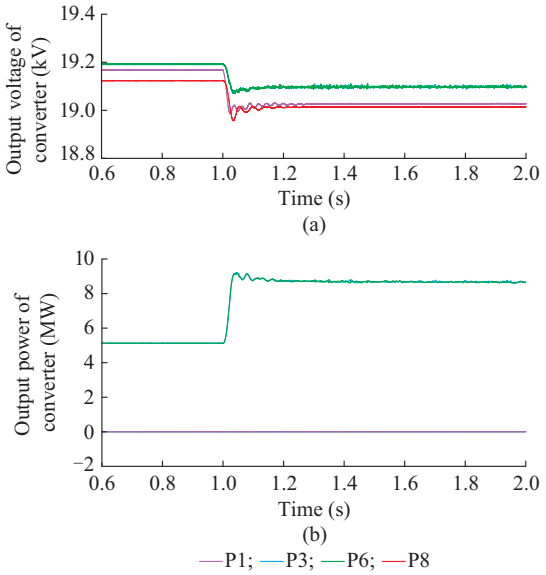

Fig. 11. Simulation waveforms in off-grid voltage droop regulation mode. (a) Output voltage waveforms. (b) Output power waveforms.

B. Mode Switching Control Simulation

To ensure the fairness of our comparisons, the control parameters of the regulators in NMSM are set to be consistent with those in TVMC. In TVMC, three PI regulators (PI1, PI2, and PI3) are utilized to control a converter station with a voltage margin controller, as shown in Fig. 6. Among these regulators, PI1 and PI3 are voltage regulators with proportional coefficients of K_{p1} = 0.001 and integral coefficients of K_{i1} = 0.13. PI2 is a power regulator with a proportional coefficient of K_{p2} = 0.12 and integral coefficient of K_{i2} = 200. When utilizing the NMSM proposed in this paper, only two regulators are required, namely the voltage regulator PI1 and power regulator PI2, as shown in Fig. 7. To make the mode switching process smoother, droop control is added to the proposed mode switching control strategy with a droop coefficient of 0.5.

Figure 12 presents dynamic waveforms during the process of switching between different voltage regulation modes. Prior to t = 1 s, all converters in the DC distribution system work under normal conditions and the system adopts the main voltage regulation mode. The AC main network converter P8 works in constant DC voltage control mode with a voltage command value of 20 kV. P1 operates in constant DC power control with a power command value of 5 MW. The maximum power values of P3 and P6 are 5 MW and 6 MW, respectively. When t = 1 s, the circuit breaker on the AC side of P8 malfunctions and the input power from P8 to the DC system drops to zero. When t = 2 s, the ±150 kV HVDC-side circuit breaker is disconnected and P1 is out of operation.

In the simulation waveforms in Fig. 12, one can clearly see the switching processes between different voltage regulation modes. Prior to t = 1 s, the system operates in the main voltage regulation mode. When t = 1 s, P8 malfunctions, causing a system power imbalance followed by a drop in the DC bus voltage. When the DC bus voltage drops to 19.64 kV, P1 begins to take over the control of the DC bus voltage and switches to backup voltage regulation mode. After 0.35 s, the system operates stably at a new operation point with a stable bus voltage of 19.6 kV. When t = 2 s, the power exchange between P1 and P8 and ±10 kV MVDC distribution network is zero and the operation point in the backup voltage regulation mode begins to shift. When the DC bus voltage drops to 19.28 kV, the control strategy for the system is switched from the backup voltage regulation mode to the off-grid voltage droop regulation mode, where the DC bus voltage is controlled simultaneously by the renewable energy generation units P3 and P6. During this process, the maximum power of the renewable energy generation units is predicted to be insufficient to support the entire network load, so the ES unit is switched from the previous state of charging to discharging to provide power support for the DC system. After 0.175 s, the system switches to a new steady state. From Fig. 10, it can be seen that DC bus voltage can be maintained at a constant value and that the system power balance can be guaranteed when switching between different voltage regulation modes.

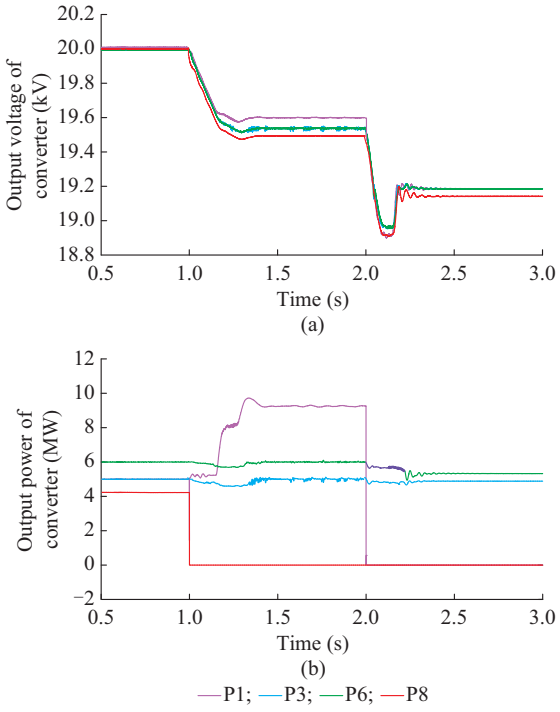

Fig. 12. Simulation waveforms when switching between different voltage regulation modes. (a) Output voltage waveforms. (b) Output power waveforms.

To demonstrate the superiority of NMSM based on a voltage coefficient proposed in this paper, comparisons between TVMC and NMSM are provided below based on simulations.

For the sake of simplicity, only the voltage waveform at a single point in the DC distribution network is considered. When the range of DC bus voltage is between $U_{dc,\mathrm{ref}}-\Delta u$ and $U_{dc,\mathrm{ref}}+\Delta u$, the NMSM utilizes droop control, which makes

the transient process of switching noticeably smoother. To keep the system at the same steady-state operation point following transient processes under the control strategies of NMSM and TVMC, the switching of NMSM in the simulation presented in this paper occurs slightly earlier than that of TVMC. For the sake of fairness, we also present a secondary comparative simulation in which switching occurs at the same time. For the sake of distinction, the TVMC that is switched at the same time as the NMSM strategy is called TVMC1, while the other is called TVMC2. The main parameters of the simulation system under NMSM and TVMC are listed in Table II.

TABLE II
MAIN PARAMETERS FOR COMPARATIVE SIMULATIONS

Method	Parameter	Value (kV)
TVMC1	Rated DC voltage $U_{dc,ref}$	20
	Lower and upper limits of reference voltage	19.6, 20.4
TVMC2	Rated DC voltage $U_{dc,ref}$	20
	Lower and upper limits of reference voltage	19.64, 20.36
NMSM	Rated DC voltage $U_{dc,ref}$	20
	Lower and upper voltages of switching point in backup voltage regulation mode	19.64, 20.36
	Switching threshold Δu in backup voltage regulation mode	0.36
	Lower and upper limits of voltage reference value in backup voltage regulation mode	19.6, 20.4
	Lower and upper voltages of switching point in droop voltage regulation mode	19.24, 20.72
	Switching threshold Δu in droop voltage regulation mode	0.74
	Lower and upper limits of voltage reference value in droop voltage regulation mode	19.2, 20.8

The waveforms of the DC bus voltage and output power values of some converters under TVMC and NMSM are presented in Fig. 13. From Fig. 13, it can be seen that the DC bus voltage and output power provided by NMSM are better than those provided by TVMC for both TVMC1 and TVMC2.

Since the NMSM avoids waiting for the relative magnitudes of the outputs of PI regulators to change, the proposed system allows other converters to take over voltage control more quickly when voltage control is lost, i.e., the fluctuations of DC bus voltage and power are smaller and the system can also be stabilized more rapidly. Comparisons of different values for TVMC and NMSM are listed in Table III. NMSM provides the advantages of fast and smooth transitions between operation modes.

C. Experimental Results

To verify the correctness of NMSM, we construct a low-voltage low-power DC distribution system in a dynamic simulation experimental platform. The schematic diagram of the platform is presented in Fig. 14. In this experiment, two DC voltage grades of 600 V and 320 V are considered to simulate medium-voltage (±10 kV) and low-voltage (±750 V) conditions, respectively. During normal operation, the power electronic traction transformer (PETT) utilizes constant DC voltage control to maintain the stability of the 320 V DC bus 2 and the DC solid state transformer (DCSST) utilizes constant DC voltage control to maintain the stability of the 600 V DC bus 1. The AC/DC converter utilizes constant DC power control.

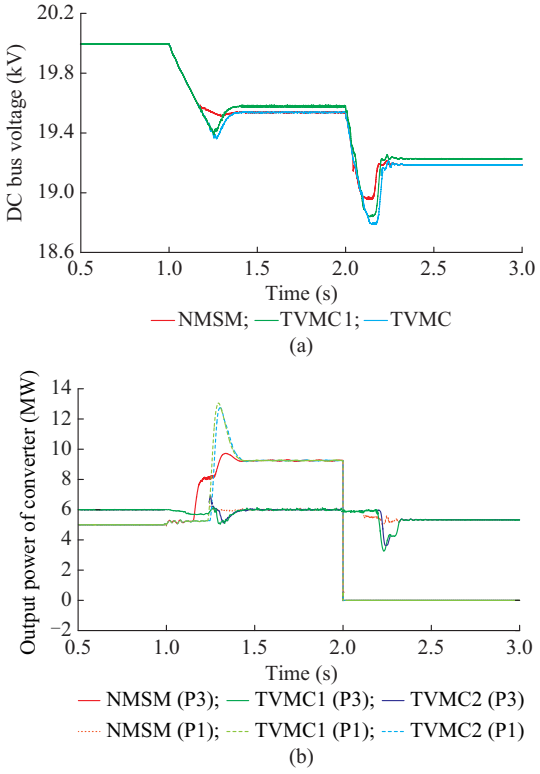

Fig. 13. Transient simulation waveforms when switching from main voltage regulation mode to backup voltage regulation mode. (a) DC bus voltage waveforms. (b) Output power waveforms.

TABLE III
COMPARISONS OF TVMC AND NMSM

Method	Voltage fluctuation (%)	Power fluctuation (%)	Transient time (s)
TVMC1	0.97	37.60	0.40
TVMC2	1.38	37.40	0.42
NMSM	0.15	4.20	0.36

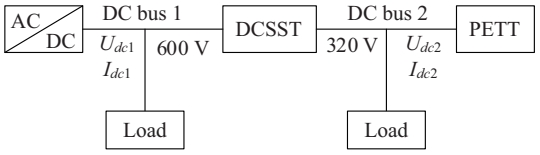

Fig. 14. Schematic diagram of experimental platform.

Figures 15 and 16 present the transient experimental waveforms when switching from main voltage regulation mode to backup voltage regulation mode. In Fig. 15, the power provided by the AC/DC converter does not meet the load power requirement on DC bus 1 on the 600 V side during normal operation (condition 1), so PETT transmits energy to the 600 V DC bus through DCSST. When DCSST is out of opera-

tion, the 600 V DC bus voltage U_{dc1} drops based on the resulting power imbalance.

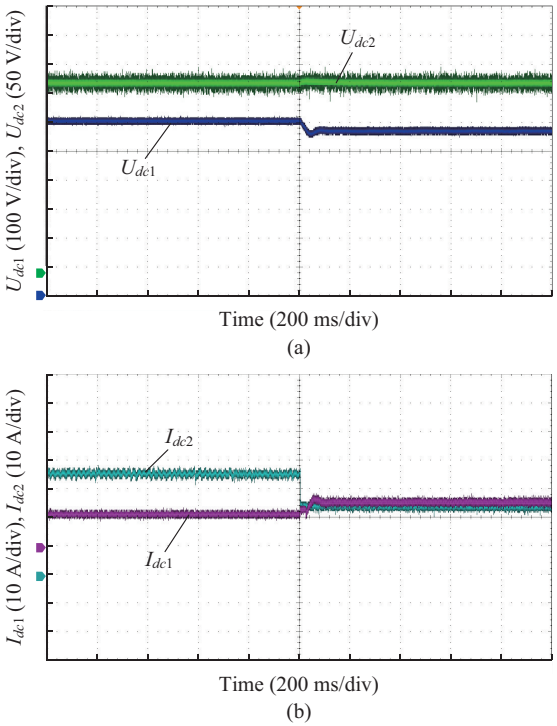

Fig. 15. Transient experimental waveforms when switching from main voltage regulation mode to backup voltage regulation mode under condition 1. (a) DC voltage waveforms. (b) DC current waveforms.

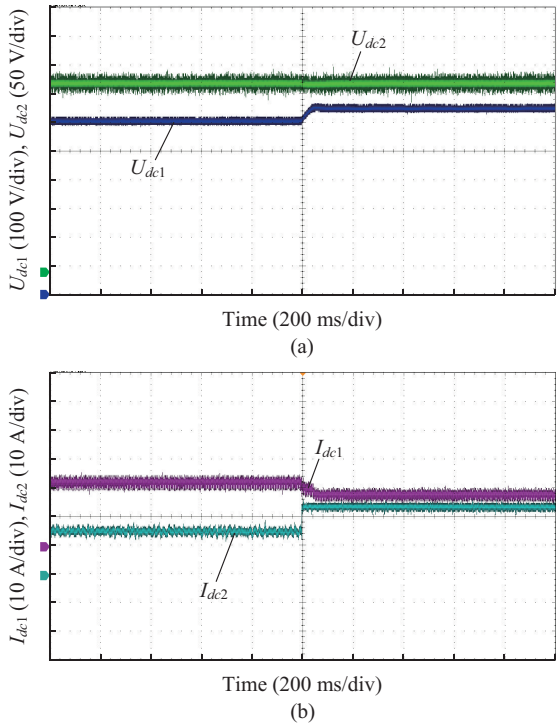

Fig. 16. Transient experimental waveforms when switching from main voltage regulation mode to backup voltage regulation mode under condition 2. (a) DC voltage waveforms. (b) DC current waveforms.

From the experimental results shown in Fig. 15, it can be seen that when DCSST is out of operation and the DC bus 1 voltage drops to 560 V, the AC/DC converter begins to take over control of the DC bus voltage and acts as a new slack bus for DC bus 1. The output current (output power) I_{dc1} of the AC/DC converter increases and the output current (output power) I_{dc2} of PETT decreases to meet the load demands of the DC buses on both sides.

In Fig. 16, the AC/DC converter provides more power than the 600 V DC bus load power requirement during normal operation (condition 2), so the AC/DC converter transmits energy to the 320 V DC bus through DCSST. When DCSST is out of operation, the 600 V DC bus voltage increases based on the resulting power imbalance. When the mode switching control strategy proposed in this paper is used, the output current (output power) I_{dc1} of the AC/DC converter decreases and the output current (output power) I_{dc2} of PETT increases, allowing the voltage of DC bus 1 to be stabilized at 640 V while the voltage of DC bus 2 U_{dc2} is continuously maintained at 320 V.

Figures 15 and 16 shows that, during the transient processes, NMSM can achieve fast and smooth voltage takeover in the event of converter station faults.

VI. Conclusion

In this paper, a fast mode switching method based on a voltage coefficient is proposed for a typical ring DC distribution system with multiple voltage levels. The main contributions of this paper are stated below.

1) According to the voltage regulation capability of the converter station and the DC bus voltage range, different voltage regulation modes are implemented to ensure that the DC bus voltage stability and power balance are maintained under different operation conditions.

2) The disadvantages of long transition time and large fluctuations in voltage and power during mode switching under TVMC are analyzed theoretically. Based on the results, the NMSM based on a voltage coefficient is proposed. By introducing a voltage coefficient associated with DC bus voltage deviations, different voltage regulation modes can realize automatic switching based on local information without the communication between devices.

3) The effectiveness of three voltage regulation modes and NMSM is verified utilizing a simulation platform. The fast mode switching method based on a voltage coefficient proposed in this paper is compared to TVMC based on simulations. The simulation results reveal that compared to TVMC, NMSM based on a voltage coefficient has less DC voltage overshoot and lower power impulses during the switching process of the voltage regulation mode. Additionally, the proposed system can reach a new stable operation point more quickly.

4) An experimental platform is constructed to verify the validity and feasibility of the NMSM.

The control strategy proposed in this paper can effectively solve the complex switching problems of converter station working modes related to switching between operation modes in a DC power distribution system. The generation of

overcurrent in the line is reduced, and the steady-state and transient operation characteristics of a multi-terminal flexible DC distribution system can be improved. The proposed method has wide adaptability and scalability.

REFERENCES

[1] K. Tan, P. So, Y. Chu *et al*., "Coordinated control and energy management of distributed generation inverters in a microgrid," *IEEE Transactions on Power Delivery*, vol. 28, no. 2, pp. 704-713, Apr. 2013.

[2] A. Gomez-Exposito, J. M. Mauricio, and J. M. Maza-Ortega, "VSC-based MVDC railway electrification system," *IEEE Transactions on Power Delivery*, vol. 29, no. 1, pp. 422-431, Feb. 2014.

[3] P. Kankanala, S. C. Srivastava, A. K. Srivastava *et al*., "Optimal control of voltage and power in a multi-zonal MVDC shipboard power system," *IEEE Transactions on Power Systems*, vol. 27, no. 2, pp. 642-650, May 2012.

[4] A. Huang, M. L. Crow, G. T. Heydt *et al*., "The future renewable electric energy delivery and management (FREEDM) system: the energy internet," *Proceedings of the IEEE*, vol. 99, no. 1, pp. 133-148, Feb. 2011.

[5] M. Stieneker, J. Butz, S. Rabiee *et al*., "Medium-voltage DC research grid aachen," in *Proceedings of the 2015 International ETG Congress*, Bonn, Germany, Nov. 2015, pp. 549-555.

[6] D. Boroyevich, I. Cvetković, D. Dong *et al*., "Future electronic power distribution systems a contemplative view," in *Proceedings of the 2010 12th International Conference on Optimization of Electrical and Electronic Equipment*, Basov, Romania, May 2010, pp. 1369-1380.

[7] C. Long, J. Wu, K. Smith *et al*., "MVDC link in a 33 kV distribution network," in *Proceedings of CIRED*, Beijing, China, Jun. 2017, pp. 1308-1312.

[8] K. Rudion, A. G. Orths, and P. B. Eriksen, "Offshore power system operation planning considering energy market schedules," *IEEE Transactions on Sustainable Energy*, vol. 4, no. 3, pp. 725-733, Jul. 2013.

[9] W. Lu and B. T. Ooi, "Optimal acquisition and aggregation of offshore wind power by multiterminal voltage-source HVDC," *IEEE Power Engineering Review*, vol. 18, no. 1, pp. 201-206, Feb. 2003.

[10] T. Nakajima and S. Irokawa, "A control system for HVDC transmission by voltage sourced converters," in *Proceedings of the 1999 IEEE PES Summer Meeting*, Edmonton, Canada, Jul. 1999, pp. 1113-1119.

[11] W. Wang and M. Barnes, "Power flow algorithms for multi-terminal VSC-HVDC with droop control," *IEEE Transactions on Power Systems*, vol. 29, no. 4, pp. 1721-1730, Jul. 2014.

[12] T. M. Haileselassie and K. Uhlen, "Impact of DC line voltage drops on power flow of MTDC using droop control," *IEEE Transactions on Power Systems*, vol. 27, no. 3, pp. 1441-1449, Aug. 2012.

[13] L. Xu and L.Yao, "DC voltage control and power dispatch of a multi-terminal HVDC system for integrating large offshore wind farms," *IET Renewable Power Generation*, vol. 5, no. 3, pp. 223-233, Jun. 2011

[14] Z. Wang, K. Li, J. Ren *et al*., "A coordination control strategy of voltage-source-converter-based MTDC for offshore wind farms," *IEEE Transactions on Industry Applications*, vol. 51, no. 4, pp. 2743-2752, Jul. 2015.

[15] M. Li, X. Liu, and P. Chen, "Fast voltage margin control strategy for VSC-MTDC systems," *Power System Technology*, vol. 40, no. 10, pp. 3045-3051, Oct. 2016.

[16] F. Gao, R. Kang, J. Cao *et al*., "Primary and secondary control in DC microgrids: a review," *Journal of Modern Power Systems and Clean Energy*, vol. 7, no. 2, pp. 227-242, Mar. 2019.

[17] L. Qiao, X. Li, D. Huang *et al*., "Coordinated control for medium voltage DC distribution centers with flexibly interlinked multiple microgrids," *Journal of Modern Power Systems and Clean Energy*, vol. 7, no. 3, pp. 599-611, May 2019.

[18] J. Zhang, J. Liu, J. Yang *et al*., "An LLC-LC type bidirectional control strategy for LLC resonant converter in power electronic traction transformer," *IEEE Transactions on Industrial Electronics*, vol. 65, no. 11, Nov. 2018, pp. 8595-8604.

[19] J. Xu and J. Xie, "LCL-resonance damping strategies for grid-connected inverters with LCL filters: a comprehensive review," *Journal of Modern Power Systems and Clean Energy*, vol. 6, no. 2, pp. 292-305, Mar. 2018.

Jianqiang Liu received the B.S. and Ph.D. degrees in electrical engineering from Beijing Jiaotong University, Beijing, China, in 2003 and 2008, respectively. Currently, he is a professor in the School of Electrical Engineering, Beijing Jiaotong University, Beijing, China. His research work is related to electric energy conversion, control of AC machines, and traction drive system.

Xiaoguang Huang received the B.S. and M.S. degrees in electrical engineering from Beijing Jiaotong University, Beijing, China, in 2001 and 2006, respectively, where he is currently working toward the Ph.D. degree. His research interests include optimal dispatch of power system, smart grids and energy hubs.

Ying Hong received the B.S. degree in electrical engineering from Yanshan University, Qinhuangdao, China. She is currently working toward the M.S. degree in power electronics with the School of Electrical Engineering, Beijing Jiaotong University, Beijing, China. Her research interest is flexible DC distribution network.

Zuyi Li received the B. S. degree from Shanghai Jiao Tong University, Shanghai, China, in 1995, the M.S. degree from Tsinghua University, Beijing, China, in 1998, and the Ph. D. degree from the Illinois Institute of Technology (IIT), Chicago, USA, in 2002, all in electrical engineering. He is currently a professor with the Electrical and Computer Engineering Department, IIT, Chicago, USA. His research interests include economic and secure operation of electric power systems, cyber security in smart grid, renewable energy integration, electric demand management of data centers, and power system protection.